Published in final edited form as:

Math Med Biol. 2022 February 22; 39(1): 77–104. doi:10.1093/imammb/dqab018.

## A multi-scale/multi-physics model for the theoretical study of the vascular configuration of retinal capillary plexuses based on OCTA data

#### Greta Chiaravalli\*,

Department of Physics, Politecnico di Milano, Milan 20133, Italy, Italian Institute of Technology, Milan 20133, Italy

#### Giovanna Guidoboni,

Department of Electrical Engineering and Computer Science, Department of Mathematics, University of Missouri, Columbia, MO 65211, USA

#### Riccardo Sacco,

Department of Mathematics, Politecnico di Milano, Milan20133, Italy

#### Jake Radell,

Department of Ophthalmology, Icahn School of Medicine at Mount Sinai, New York, NY 10029, USA

#### **Alon Harris**

Department of Ophthalmology, Icahn School of Medicine at Mount Sinai, New York, NY 10029,

#### **Abstract**

The retinal tissue is highly metabolically active and is responsible for translating the visual stimuli into electrical signals to be delivered to the brain. A complex vascular structure ensures an adequate supply of blood and oxygen, which is essential for the function and survival of the retinal tissue. To date, a complete understanding of the configuration of the retinal vascular structures is still lacking. Optical coherence tomography angiography has made available a huge amount of imaging data regarding the main retinal capillary plexuses, namely the superficial capillary plexuses (SCP), intermediate capillary plexuses (ICP) and deep capillary plexuses (DCP). However, the interpretation of these data is still controversial. In particular, the question of whether the three capillary plexuses are connected in series or in parallel remains a matter of debate. In this work, we address this question by utilizing a multi-scale/multi-physics mathematical model to quantify the impact of the two hypothesized vascular configurations on retinal hemodynamics and oxygenation. The response to central retinal vein occlusion (CRVO)

Conflict of Interests

<sup>\*</sup>Corresponding author: greta.chiaravalli@polimi.it.

Alon Harris would like to disclose that he received remuneration from Adom, Qlaris and Luseed for serving as a consultant and he serves on the board of Adom, Qlaris and Phileas Pharma. Prof. Harris holds an ownership interest in AdOM, Luseed, Oxymap, Qlaris, Phileas Pharma and QuLent. All relationships listed above are pursuant to Icahn School of Medicine's policy on outside activities. Giovanna Guidoboni would like to disclose that she received remuneration from Foresite Healthcare LLC for serving as a consultant. This relationship is pursuant to University of Missouri's policy on outside activities.

and intraocular pressure (IOP) elevation is also simulated depending on whether the capillary plexuses are connected in series or in parallel. The simulation results show the following: (i) in the in series configuration, the plexuses exhibit a differential response, with DCP and ICP experiencing larger pressure drops than SCP; and (ii) in the in parallel configuration, the blood flow redistributes uniformly in the three plexuses. The different vascular configurations show different responses also in terms of oxygen profiles: (i) in the in series configuration, the outer nuclear layer, outer plexiform layer and inner nuclear layer (INL) are those most affected by CRVO and IOP elevation; and (ii) in the in parallel configuration the INL and ganglion cell layer are those most affected. The in series results are consistent with studies on paracentral acute middle maculopathy, secondary to CRVO and with studies on IOP elevation, in which DCP and ICP and the retinal tissues surrounding them are those most affected by ischemia. These findings seem to suggest that the *in series* configuration better describes the physiology of the vascular retinal capillary network in health and disease.

#### **Keywords**

retina; capillary plexuses; vascularization; oxygenation; intraocular pressure elevation; central retinal vein occlusion; optical coherence tomography angiography

#### 1. Introduction

In order to serve its function of transducing light into neural signals and thereby providing humans with a sense of vision, it is essential that the retina maintains adequate blood flow at all times. Furthermore, as a highly metabolically active tissue, retinal oxygen and nutrient demands are quite high; even small reductions in blood flow can have devastating effects on the eye (Yu & Cringle, 2001). Despite the clinical importance of retinal blood flow to sight, many questions about the basic anatomy and physiology of the retinal capillaries still remain unsolved. Enhancing the scientific community's understanding of these capillaries may prove key in further elucidating the pathophysiology underlying diseases of retinal ischemia, especially paracentral acute middle maculopathy (PAMM) and central retinal vein occlusion (CRVO).

In recent years, a new noninvasive technique known as optical coherence tomography angiography (OCTA) has been extensively utilized to study the deep vascular layers of the retina. This technique allows for imaging of the retinal vasculature with high depth resolution, which provides numerous details on the complex anatomy of the retinal microvasculature (Lavia *et al.*, 2020). OCTA studies have identified three main distinct capillary plexuses:

- **SCP** or **SVP**, *superficial capillary* or *vascular plexus*, primarily located in the ganglion cell layer;
- **ICP**, *intermediate capillary plexus*, located between the inner nuclear layer (INL) and the inner plexiform layer, in the middle retina region, it is robust in the fovea but is not present in the retinal periphery;

• **DCP**, *deep capillary plexus*, located above the outer plexiform layer (OPL), often considered, together with the ICP, to compose the deep capillary complex; ICP and DCP are separated by the INL, which in the peripheral retina is so thin that does not allow the two plexuses to be separately visualized.

Despite the introduction of OCTA, the spatial and functional relationships between the various capillary plexuses are still poorly understood. In particular, two main hypotheses regarding the plexuses' connections have been proposed, as illustrated in Fig. 1:

- In parallel configuration: Campbell et al. (2017) proposed a model of three microvascular plexuses where SCP, ICP and DCP are arranged in a hammock-like configuration, each communicating through vertically oriented arterioles and veins:
- *In series* configuration: Fouquet *et al.* (2017) proposed a consecutive organization of the capillary plexuses, where the DCP serves as the main venous drainage, consistent with other studies (Garrity *et al.*, 2017; Paques *et al.*, 2003).

As research into retinal vasculature configuration continues to develop, an increasing body of evidence seems to point towards primary in series flow with minor in parallel elements (Scharf et al., 2018). One of the strongest arguments for this arrangement is the functional role of the DCP, which seems to primarily be one of venous drainage. Recently, an OCTA study of 14 healthy volunteer eyes examined the shortest path of flow between arteries and veins and found that all flow coursed through the DCP (Cabral et al., 2020). No drainage came strictly from the SCP without first flowing to the ICP/DCP, strongly supporting the in series model. Furthermore, an OCTA study of 23 patients with retinal vein occlusion showed that in this pathogenic state, all newly formed collateral vessels ultimately drained via the DCP (Freund et al., 2018). The same study found that none of these collateral vessels were confined exclusively to the SCP, indicating that they may function to increase flow from the SCP to the ICP and DCP, where drainage could occur. In addition to functional OCTA evidence pointing towards in series flow, there have also been structural studies using confocal microscopy to examine the connections between the retinal plexuses. Initial confocal imaging studies indicated that blood flow between plexuses is partly in series and partly in parallel (Chandrasekera et al., 2018). Subsequent work showed that arterioles typically directly fed the SCP and rarely directly fed the ICP, indicating predominant in series flow, with a minor in parallel component (Yu et al., 2019). Arterioles never directly fed the DCP; all DCP flow originated in the ICP, indicating pure in series organization between ICP and DCP. Venous outflow was present in all three plexuses but was most robust in the DCP.

To help resolve the debate concerning the structural and functional relationships among the retinal vascular plexuses, we propose in this study a theoretical approach based on a multi-scale and multi-physics description of retinal hemodynamics and oxygenation that can be used as a virtual laboratory to compare the two hypothesized vascular configurations. The paper is organized as follows. The proposed multi-scale/multi-physics modelling approach to retinal physiology is outlined in Section 2, with the details about hemodynamics and oxygenation provided in Sections 3 and 4, respectively. Results are presented in Section

5, where the response to CRVO and intraocular pressure (IOP) elevation is simulated depending on whether the capillary plexuses are connected *in series* or *in parallel*. The results are discussed in Section 6 and conclusions and future perspectives are summarized in Section 7.

# 2. A multi-scale and multi-physics modelling approach to retinal physiology

Retinal physiology is characterized by an intrinsic *multi-scale* and *multi-physics* nature. Of particular relevance for this paper are the multi-scale aspects related to the dimensions of blood vessels, whose diameters range from 130 to 150  $\mu$ m in the central retinal artery (CRA) and vein to approximately 5  $\mu$ m in the capillaries (Arciero *et al.*, 2013; Goldenberg *et al.*, 2013), and the multi-sphysics aspects related to hemodynamics and oxygenation, whose complex interplay is essential to sustain the retinal function. As a consequence, the multi-scale/multi-physics model for retina physiology proposed in this article consists of the following two main blocks:

- (M1) the **retinal hemodynanic model** (see Section 3), which describes retinal hemodynamics at the micro-, meso- and macro-scale;
- (M2) the retinal oxygenation model (see Section 4), which describes the diffusion and consumption of oxygen across the various retinal tissue layers.

Fig. 2 schematically illustrates the overall multi-scale/multi-physics modelling approach. Within model block M1 the information from the micro-scale level is used as an input for the meso-scale level, which in turn serves as an input for the the macro-scale level, as indicated by the vertical purple arrows in Fig. 2. The output of model block M1 is then used as an input for the numerical simulation of retinal tissue oxygenation based on model block M2, as indicated by the horizontal purple arrows in Fig. 2. The resulting interaction among the model blocks is, therefore, a *one-way coupling* approach between the simulations of retinal hemodynamics and oxygenation.

## 3. M1: mathematical model of retinal hemodynamics

The multi-scale model for retinal hemodynamics adopted here stems from the formulation proposed in Guidoboni *et al.* (2014b), which comprises five main compartments: the CRA, arterioles, capillaries, venules and the central retinal vein (CRV). The model is based on the electrical circuit analogy illustrated in Fig. 3 in which three levels of investigation are identified: micro-, meso- and macro-scale levels. Each level is going to be described in detail in the next sections.

#### 3.1 Micro-scale level

Let us introduce the subscripts p and s to denote quantities related to the *in parallel* and *in series* configurations, respectively, and the subscripts SCP, ICP and DCP to denote the quantities related to the superficial, intermediate and deep capillary plexuses, respectively. Furthermore, let us denote by  $\mathscr C$  the set of subscripts  $\mathscr C = \{SCP, ICP, DCP\}$ . This notation will be adopted throughout the article. Fig. 4 shows how the data contained in an OCTA image

(panel A) are treated through a segmentation process (panel B) to obtain as an output a map of the occupied/non occupied distribution of capillaries within the OCTA image (panel C).

In Campbell *et al.* (2017), the capillary density  $\gamma_i$  for each capillary plexus,  $i \in \mathcal{C}$ , is defined as the ratio between the area occupied by the capillaries,  $A_{\text{cap},i}$ , and the total area of the image obtained via OCTA,  $A_{\text{tot},i}$ , namely

$$\gamma_i := \frac{A_{\text{cap}, i}}{A_{\text{tot}, i}}, \quad \text{for } i \in \mathscr{C}.$$
(3.1)

The values reported in Campbell *et al.* (2017) for each capillary plexus are  $\gamma_{SCP} = 0.28$ ,  $\gamma_{ICP} = 0.22$  and  $\gamma_{DCP} = 0.13$ . We proceed by making the following assumptions:

(A1) every OCTA image has the same size  $A_{\text{tot},i} = A_{\text{tot}}$ , for  $i \in \mathcal{C}$ ;

(A2) every capillary in each capillary plexus (SCP, ICP and DCP) has the same length  $L_{\rm cap}$  and same diameter  $D_{\rm cap}$ . Thus, utilizing Poiseuille's flow model (Sacco et al., 2019, Chapter 15) with a constant blood viscosity  $\mu$  yields the following expression for the resistance of a single capillary:

$$R_{\rm cap} = \frac{128\mu L_{\rm cap}}{\pi D_{\rm cap}^4};$$
 (3.2)

(A3) the total area  $A_{\text{tot}}$  of each OCTA image is subdivided into  $N_{tot}$  rectangles; each rectangle has area equal to  $L_{\text{cap}}D_{\text{cap}}$ . Thus, we can write

$$\gamma_{i} = \frac{A_{\text{cap}_{i}}}{A_{\text{tot}}} = \frac{N_{\text{cap}_{i}} L_{\text{cap}} D_{\text{cap}}}{N_{tot} L_{\text{cap}} D_{\text{cap}}} = \frac{N_{\text{cap}_{i}}}{N_{tot}} i \in \mathscr{C};$$
(3.3)

(A4) within each capillary plexus, the capillaries are arranged in parallel. Thus, an equivalent resistance  $R_{\text{eq},i}$ , for  $i \in \mathcal{C}$ , can be defined as

$$R_{\text{eq}, i} = \frac{R_{\text{cap}}}{N_{\text{cap}_i}} = \frac{N_{tot}}{N_{\text{cap}_i}} \frac{R_{\text{cap}}}{N_{tot}} = \frac{R_{\text{cap}}}{\gamma_i N_{tot}} \quad i \in \mathcal{C};$$
(3.4)

(A5) the capillary densities estimated via OCTA does not capture the totality of the complex 3D capillary architecture, which in addition might differ depending on whether the capillary plexuses are connected in series or in parallel. Thus, we introduce a correction factor  $\lambda_j$ , for j = s, p, so that we can write

$$R_{i,j} = \lambda_i R_{\text{eq},i} \quad i \in \mathcal{C}, j = s, p, \tag{3.5}$$

where now  $R_{i,j}$  represents an effective resistance of the capillary plexus i in the configuration j. The value of the correction factor  $\lambda_j$ , for j = s, p, will be determined when, in the next sections, the micro-scale level will be connected to the meso- and macro-scale. To this end, it is instrumental to rewrite relation (3.4) in the equivalent form

$$R_{i,j} = R_{\text{cap}} \frac{\delta_j}{\gamma_i} \quad i \in \mathcal{C}, j = s, p,$$
(3.6)

where

$$\delta_j := \frac{\lambda_j}{N_{tot}} \quad j = s, p. \tag{3.7}$$

#### 3.2 Meso-scale level

The meso-scale level connects the micro-scale description of the capillary plexuses, which is embodied in the expression (3.6) for the effective resistance  $R_{i,j}$  of the capillary plexus  $i \in \mathcal{C}$  in the configuration j = s, p, with the macro-scale description of the retinal circulation, which is represented by the macro-scale capillary resistance  $R_7$  in the electric equivalent network of Fig. 3. Denoting by  $\overline{U}$  the reference value of any macro-scale variable U, we indicate by  $\overline{R}_7$  the reference value for  $R_7$ .

In the *in parallel* configuration the inverse of the total equivalent resistance is equal to the sum of the reciprocals of the resistances of each capillary plexus, namely

$$\frac{1}{\overline{R}_{7}} = \frac{1}{R_{\text{SCP}, p}} + \frac{1}{R_{\text{ICP}, p}} + \frac{1}{R_{\text{DCP}, p}} = \sum_{i \in \mathcal{C}} \frac{1}{R_{i, p}}.$$
(3.8)

The expression of  $R_{i,j}(3.6)$  is substituted into (3.8) yielding to

$$\delta_p = \frac{\overline{R}_7}{R_{\text{cap}}} \sum_{q \in \mathcal{L}} \gamma_q, \tag{3.9}$$

from which, using again (3.6), we get

$$R_{i, p} = \overline{R}_{7} \gamma_{i}^{-1} \left( \sum_{q \in \mathscr{C}} \gamma_{q} \right) \quad i \in \mathscr{C}.$$
(3.10)

In the *in series* configuration the SCP is assumed to be in direct contact with the arterioles and the DCP is assumed to be the main venous drain of the retinal microvasculature (Garrity *et al.*, 2017; Paques *et al.*, 2003). In this case, the total equivalent resistance is equal to the sum of the resistances of each capillary plexus, namely

$$\overline{R}_7 = R_{\text{SCP}, s} + R_{\text{ICP}, s} + R_{\text{DCP}, s} = \sum_{i = \mathscr{C}} R_{i, s}.$$
 (3.11)

The expression of  $R_{i,j}(3.6)$  is substituted into (3.11) yielding to

$$\delta_s = \frac{\overline{R}_7}{R_{\text{cap}}} \left( \sum_{q = \mathscr{C}} \gamma_q^{-1} \right)^{-1},\tag{3.12}$$

from which, using again (3.6), we get

$$R_{i,s} = \overline{R}_7 \gamma_i^{-1} \left( \sum_{q = \mathscr{C}} \gamma_q^{-1} \right)^{-1} \quad i = \mathscr{C}. \tag{3.13}$$

REMARK 3.1 The expressions (3.10) and (3.13) representing the properties of the capillary vasculature at the meso-scale level in the two hypothesized configurations depend on the macro-scale reference resistance  $\bar{R}_7$  and the micro-scale density ratio  $\gamma_i$ . Notably, the meso-scale resistances are not affected by the specific values of the correction factors since, ultimately, expressions (3.10) and (3.13) do not depend explicitly on  $\delta_i$ .

#### 3.3 Macro-scale level

The macro-scale description of retinal hemodynamics consists of the electric equivalent network in Fig. 3. Let us denote by  $N_{nod}$  the number of internal nodes in the circuit, with  $N_{nod} = 12$  in our case. The circles at the inlet and outlet sections of the equivalent electric circuit represent pressure sources for the systemic arterial and venous pressures, whose reference values will be denoted by  $\overline{P}_0$  and  $\overline{P}_{N_{nod}+1}$ , respectively. The pressure difference between the systemic arterial and venous pressures is the driving force of the blood flow

between the systemic arterial and venous pressures is the driving force of the blood flow through the network. The rest of the circuit consists of resistors connected in series, whose characterization is detailed next. Referring to Fig. 5, we denote the following:

- $P_a$  and  $P_b$  the nodal pressures of node a and b, respectively;
- $\Delta P = P_a P_b$  the pressure drop across *a* and *b*;
- $\hat{P} = \frac{P_a + P_b}{2}$  the average pressure experienced by the vessel;
- Othe volumetric flow rate between a and b.

The relation between  $\Delta P$  and Q is represented by the hydraulic analog of Ohm's law and reads

$$\Delta P = RQ,\tag{3.14}$$

where R is a positive quantity representing the *resistance* of the resistor connecting nodes a and b.

In the case of a linear invariant resistor (left panel in Fig. 5), R is computed using Poiseuille's model Eq. (3.2). In the case of a nonlinear resistor (right panel in Fig. 5), R depends on the nodal pressures  $P_a$  and  $P_b$  through the transmural pressure difference  $\Delta P_{tm}$  defined as

$$\Delta P_{tm} = \hat{P} - p_{\text{ext}},\tag{3.15}$$

where  $p_{\text{ext}}$  is the pressure acting from the external environment on the blood vessel. Nonlinear resistances are utilized to model the translaminar and intraocular segments of CRA and CRV and the resistances of venules; these resistances are characterized by the following constitutive equation:

$$R(\Delta P_{tm}) = \begin{cases} \frac{K_r \rho L}{A_{\text{ref}}^2} \left[ \frac{\Delta P_{tm}}{K_p k_l} + 1 \right]^{-4} & \text{if } \Delta P_{tm} \ge 0\\ \frac{K_r \rho L}{A_{\text{ref}}^2} \left[ 1 - \frac{\Delta P_{tm}}{K_p} \right]^{4/3} & \text{if } \Delta P_{tm} < 0. \end{cases}$$
(3.16)

The parameters  $K_P K_P$  and  $k_I$  are defined as

$$K_r = \frac{8\pi\mu}{\rho}, \quad K_p = \frac{Eh^3}{\sqrt{1-v^2}} \left(\frac{\pi}{A_{\text{ref}}}\right)^{3/2}, \quad k_l = \frac{12A_{\text{ref}}}{\pi h^2},$$
 (3.17)

where E, v and h are the Young modulus, the Poisson ratio and the thickness of the vessel wall, respectively;  $\rho$  is the blood density; and  $A_{\text{ref}}$  is the vessel cross-sectional area when  $\Delta P_{tm} = 0$ . In each compartment, the external pressure  $p_{\text{ext}}$  is assumed to be equal to the value of IOP. The reference values for all the pressures and resistances in the equivalent electric circuit are available in Guidoboni *et al.* (2014b) and reported in Tables 1 and 2. The values of the resistances of each capillary bed in the *in parallel* and *in series* configurations are listed in Table 3.

Remark 3.2 It is worth noticing that  $\overline{P}_{N_{nod}+1} \leq \overline{P}_n \leq \overline{P}_0$  for  $n = 1, ..., N_{nod}$ .

In order to evaluate the internal nodal pressures  $P_n$ , for  $n = 1, ..., N_{nod}$ , we write the hydraulic analog of Kirchhoff current law at each internal node n of the circuit

$$-Q_n + Q_{n+1} = 0, (3.18)$$

where the constitutive law relating the volumetric flow rate Q and the pressure difference  $\Delta P$  across the m-th branch of the circuit connecting nodes a=m-1 and b=m is expressed by Ohm's law (3.14). Replacing the expressions of  $Q_n$  and  $Q_{n+1}$  into (3.18) yields a nonlinear algebraic system of  $N_{nod}$  equations for the  $N_{nod}$  internal nodal pressures  $P_n$ ,  $n=1,\ldots,N_{nod}$ , which can be written in matrix form as

$$\underline{Y}(p)p = \underline{b}, \tag{3.19}$$

where  $\underline{\mathbf{p}} \in \mathbb{R}^{N_{nod}}$  is a column vector containing the unknown nodal pressures, the right-hand side

$$\underline{\mathbf{b}} = \left[\frac{\overline{P}_0}{R_1}, 0, \dots, 0, \frac{\overline{P}_{N_{nod}+1}}{R_{N_{nod}+1}}\right]^T$$

is a column vector of size  $N_{nod}$  accounting for the given pressure boundary values and  $\underline{\underline{\mathbf{Y}}}(\mathbf{p}) \in \mathbb{R}^{N_{nod} \times N_{nod}}$  is the admittance matrix of the network defined as

$$\underline{\underline{Y}}(\underline{\mathbf{p}}) = \begin{bmatrix} \left(\frac{1}{R_1} + \frac{1}{R_2}\right) & -\frac{1}{R_2} & 0 & \cdots & 0 & 0 \\ -\frac{1}{R_2} & \left(\frac{1}{R_2} + \frac{1}{R_3(\Delta P_3)}\right) - \frac{1}{R_3(\Delta P_3)} & \cdots & 0 & 0 \\ \vdots & \vdots & \vdots & \ddots & \vdots & \vdots \\ 0 & 0 & 0 & \cdots & -\frac{1}{R_{12}} \left(\frac{1}{R_{12}} + \frac{1}{R_{13}}\right) \end{bmatrix}$$
(3.20)

In the above matrix, all the resistances are real and positive. It can be shown that  $\underline{\underline{Y}}(\underline{p})$  is symmetric, positive definite and irreducibly diagonally dominant. For  $m = \{3, 4, 8, 9, 10, 11\}$ , the positive value  $R_m = R_m(\Delta P_{tm,m})$  of the resistance nonlinearly depends on the transmural pressure difference  $\Delta P_{tm,m} = \hat{P}_m - p_{\text{ext},m}$ , as expressed by Eq. (3.16), having set

$$\hat{P}_m = \frac{P_{m-1} + P_m}{2} \quad m = 1, ..., N_{nod} + 1, \tag{3.21}$$

and having denoted by  $p_{\text{ext},m}$  the pressure acting from the external environment on the m-th network compartment.

In order to solve the nonlinear algebraic system (3.19), we use the following fixed-point iteration: Given  $\underline{\mathbf{p}}^{(0)} \in \mathbb{R}^{N_{nod}}$ ,  $\forall k \geq 0$  until convergence, compute the sequence of vectors  $\{\mathbf{p}^{(k)}\}$  through the formula

$$\underline{\mathbf{p}}^{(k+1)} = T(\underline{\mathbf{p}}^{(k)}) \quad k \ge 0, \tag{3.22}$$

where the iteration map  $T(\mathbf{x})$  is

$$T(\mathbf{\underline{x}}) = [\mathbf{\underline{Y}}(\mathbf{x})]^{-1}. \tag{3.23}$$

Remark 3.3 Each step of the fixed-point iteration (3.22) is well posed because matrix  $\underline{\underline{\mathbf{Y}}}(\underline{\underline{\mathbf{p}}}^{(k)})$  is invertible.

The fixed-point iteration (3.22) can be efficiently implemented via the Thomas Algorithm, which solves at each step  $k \ge 0$  the tridiagonal linear system at a computational cost of  $(8N_{nod}-7)$  floating-point operations (Quarteroni *et al.*, 2007). The fixed-point iteration is stopped at the first value  $k^* \ge 0$  of the iteration counter k such that the following termination criterion is satisfied:

$$\left\|\mathbf{p}^{(k^*+1)} - \mathbf{p}^{(k^*)}\right\|_{\infty, h} < \epsilon, \tag{3.24}$$

where  $\epsilon = 10^{-6}$  mmHg and

$$\|\mathbf{x}\|_{\infty, h} = \max_{q = 1, ..., N_{nod}} |x_q| \quad \forall \mathbf{x} \in \mathbb{R}^{N_{nod}}.$$

The initial guess  $\underline{\mathbf{p}}^{(0)}$  for the internal pressure values has been set equal to the reference values reported in Table 2. Thanks to the properties of  $\mathbf{Y}$  and Remark 3.2, the discrete maximum principle holds, i.e. for each  $k \ge 0$  we have

$$P_0 \le P_n^{(k)} \le P_{N_{nod}+1} \quad n = 1, ..., N_{nod}.$$
 (3.25)

The fact that the computational algorithm (3.22) satisfies at each iteration the discrete maximum principle confers to the computed solution a sound biophysical reliability since (3.25) indicates that the nodal pressures in the circuit will remain in the range between the systemic arterial and venous pressures.

**3.3.1 Post-processing in the capillary district.**—Let us denote by  $P_n^* := P_n^{(k^*)}$ , for  $n = 1, ..., N_{nod}$ , the pressure values computed by solving the nonlinear algebraic system (3.19) and let  $\Delta P_{\text{cap}}^* := P_6^* - P_7^*$  denote the pressure drop across the capillary compartment.

In the *in parallel* configuration, the volumetric blood flow rate  $Q_{i,p}$  streaming across each capillary plexus,  $i = \mathcal{C}$ , is

$$Q_{i,p}^* = \frac{\Delta P_{\text{cap}}^*}{R_{i,p}} = \frac{\Delta P_{\text{cap}}^*}{\overline{R}_7} \frac{\gamma_i}{\sum_{q = \mathscr{C}} \gamma_q} = Q^* \frac{\gamma_i}{\sum_{q = \mathscr{C}} \gamma_q} \quad i \in \mathscr{C}, \tag{3.26}$$

where  $Q^*$  is the volumetric blood flow rate streaming across the network of Fig. 3, computable, for instance, as

$$Q^* = \frac{\overline{P}_0 - P_1^*}{\overline{R}_1} \,. \tag{3.27}$$

In the *in series* configuration, the pressure drop  $\Delta P_{i,s}^*$  across each capillary plexus,  $i = \mathcal{C}$ , is

$$\Delta P_{i,s}^* = R_{i,s} Q^* = \Delta P_{\text{cap}}^* \left( \gamma_i \sum_{q = \mathscr{C}} \gamma_q^{-1} \right)^{-1} \quad i \in \mathscr{C}.$$
 (3.28)

The values of  $Q_{i,p}^*$  computed using (3.26) and the values of  $\Delta P_{i,s}^*$  computed using (3.28) are listed in Table 4. Numerical results obtained by running the algorithm described in Section 3.3 starting from the reference condition illustrated there yield  $\Delta P_{\text{cap}}^* = 7.9$  and  $Q^* = 6.95 \cdot 10^{-4} \text{ mL s}^{-1}$ . It is easily verified that the sum of  $Q_{i,p}^*$  in the left column of Table 4 equals  $Q^*$  and the sum of  $\Delta P_{i,s}^*$  in the right column of Table 4 equals  $\Delta P_{\text{cap}}^*$ .

Remark 3.4 Assume that  $\gamma_i = \overline{\gamma}$  for each  $i = \mathscr{C}$ . Then,

$$Q_{i,\,p}^* = Q^* \frac{\overline{\gamma}}{\sum_{q = \mathcal{C}} \overline{\gamma}} = \frac{Q^*}{3} \quad i \in \mathcal{C},$$

as expected in the case of a parallel connection of three resistors having the same resistance. Similarly,

$$\Delta P_{i,s}^* = \Delta P_{\text{cap}}^* \left( \overline{\gamma} \sum_{q = \mathscr{C}} \overline{\gamma}^{-1} \right)^{-1} = \frac{\Delta P_{\text{cap}}^*}{3} \quad i \in \mathscr{C},$$

as expected in the case of a series connection of three resistors having the same resistance.

## 4. M2: mathematical model of retinal oxygenation

In this section we illustrate the mathematical model describing the process of delivery and consumption of oxygen throughout the retinal tissue. Consistent with eye physiology, capillaries turn out to be the main vascular structure responsible for oxygen delivery to the tissue (Linsenmeier & Braun, 1992). Fig. 6 provides a schematic view of the process in which the oxygen supply provided by the retinal microcirculation is accounted for by source terms localized at the level of the capillary district and represented by black arrows.

The retinal tissue is subdivided into layers of different characteristic thickness. The metabolic consumption of each layer is modelled as an oxygen sink. The capillary plexuses are included in the description as sources of oxygen whereas the choroid and vitreous are included in the description as boundary conditions. A schematic of the retinal tissue layers is reported in Fig. 7 and discussed in Section 4.1.

#### 4.1 Retinal tissue layers

The geometrical representation of the retinal tissue is schematically illustrated in Fig. 7 in which the retina is modelled as a 1D domain  $\Omega_z$  along the z axis directed across the retinal thickness. The domain  $\Omega_z$  is made by the union of 7 disjoint layers  $\Omega_k$ , k = 1, ..., 7, in such a way that  $\Omega_z = \int\limits_{k=1}^{7} \Omega_k$ . Superposed to the above-mentioned partition in layers of the retinal tissue, we can see in Fig. 7 the presence of three shadowed areas  $\Omega_i$ , corresponding to the vascular zones occupied by the three capillary plexuses and identified with the index  $i = \mathcal{C}$ . Specifically, the DCP is located between the OPL and the INL, the ICP is located between the INL and the inner plexiform layer (IPL), whereas the SCP interpenetrates the ganglion cell and nerve fibre layer (GCL) layer (Campbell *et al.*, 2017). The segmentation of the layers is derived from two studies on OCTA imaging (Campbell *et al.*, 2017; Terry *et al.*, 2016) and reported in Table 5. The position and width of the vascularized region follows Campbell *et al.* (2017). The model accounts for a description of the parafoveal region, where the three capillary plexuses are distinguishable through the OCTA analysis (Campbell *et al.*, 2017). In this region, the thickness of the retina,  $t_{ret}$ , is estimated to be around 335  $\mu$ m (Terry *et al.*, 2016).

#### 4.2 Oxygen exchange in retinal tissue

The spatial distribution of oxygen inside the retinal tissue is described by the following nonlinear reaction—diffusion boundary-value problem:

$$-D\alpha \frac{d^2p(z)}{dz^2} = \mathcal{P}(z, p) \quad \text{in } \Omega_z, \tag{4.1a}$$

$$p(0) = p_{\rm ch},\tag{4.1b}$$

$$p(t_{ret}) = p_{vit}, (4.1c)$$

where the product ap represents the concentration of oxygen  $[O_2]$ , a being the oxygen solubility coefficient in the tissue and p the partial pressure of oxygen; D is the diffusivity of oxygen in the tissue; whereas  $\mathcal{P} = \mathcal{P}(z,p)$  is a net oxygen production term, nonlinearly depending on p, which takes into account oxygen consumption of the metabolic active layers and oxygen supply of the capillaries. Relations (4.1b) and (4.1c) are two boundary conditions for the reaction–diffusion equation (4.1a) and express the continuity between the partial pressure of oxygen inside the retinal tissue with the partial pressure of oxygen  $p_{\text{ch}}$  at the choroid (z = 0) and the partial pressure of oxygen  $p_{\text{vit}}$  at the vitreous ( $z = t_{rel}$ ), respectively. The reaction–diffusion boundary-value problem (4.1) was considered in Causin  $et\ al.\ (2016)$  and subsequently investigated in Chiaravalli (2018) and Verticchio Vercellin  $et\ al.\ (2021)$ .

#### 4.3 The oxygen net production term

The oxygen net production term  $\mathcal{P}$  is defined as

$$\mathcal{P}(z,p) = S(z,p) - C(z,p) \quad z \in \Omega_z, \tag{4.2}$$

where S and P are nonnegative functions representing production and consumption of oxygen in the tissue.  $\mathcal{P}$  has a piecewise characterization over the retinal tissue domain  $\Omega_Z$  depending on the specific characteristics of the various tissue layers. Specifically, recalling that  $\Omega_i$ , with  $i \in \mathcal{C}$ , denote the domain regions occupied by the capillary plexuses, we assume that

$$S(z, p) = \begin{cases} S_i(z) & z \in \Omega_i & i \in \mathcal{C}, \\ 0 & \text{elsewhere} \end{cases}$$
 (4.3)

where the production rate  $S_i = S_i(z)$  is described via a Krogh-type cylinder model, as in Arciero *et al.* (2008), Chiaravalli (2018) and Verticchio Vercellin *et al.* (2021) according to the relation

$$S_{i}(z) = c_{o} H_{D} \frac{\Delta S_{\text{sat}}(z) Q(z)}{V(z)} \quad z \in \Omega_{i} \quad i \in \mathcal{C},$$
(4.4)

where  $H_D$  is the discharge haematocrit;  $c_0$  is the carrying capacity of red blood cells at 100% saturation; Q is the volumetric blood flow rate through the capillary plexus  $\Omega_i$ ;  $\Delta S_{\text{sat}}$  is the saturation drop across the capillary plexus  $\Omega_i$ ; and V is the volume occupied by the capillary plexus  $\Omega_i$ ,  $i = \mathcal{C}$ . All the values of the parameters in (4.4) are reported in Table 6. We notice

that Q,  $\Delta S_{\rm sat}$ , and V attain different values in each of the three plexuses DCP, ICP and SCP and that Q and  $\Delta S_{\rm sat}$  also change accordingly to the considered vascular configuration. The piecewise definition of the consumption term C is based on Michaelis–Menten kinetics as follows:

$$C(z,p) = \alpha \frac{\mathcal{Q}^{\max}(z)p}{p + K_{1/2}},\tag{4.5}$$

where  $K_{1/2}$  and  $\mathcal{Q}^{\text{max}} = \mathcal{Q}^{\text{max}}(z)$  represent the  $O_2$  partial pressure at half maximum consumption and the maximum  $O_2$  consumption rate in the each layer, respectively. It is important to emphasize that the metabolic consumption (and therefore,  $\mathcal{Q}^{\text{max}}$ ) is not uniformly distributed across the tissue layers. In the inner segment of the photoreceptors (PH) in the outer retina, where the mitochondrial activity takes place, the metabolic consumption is high and set to  $\mathcal{Q}^{\text{max}} = 90 \, \text{mmHg s}^{-1}$ , while in the other layers in this region (namely, the RPE and the ONL) the metabolic consumption is considered to be negligible, so that we set  $\mathcal{Q}^{\text{max}} = 0 \, \text{mmHg s}^{-1}$ . In the inner retina, the OPL and the inner part of IPL have a higher consumption than that of the GCL and all the other inner retinal layers, so that we set  $\mathcal{Q}^{\text{max}}$  equal to 52 mmHg s<sup>-1</sup> and 26 mmHg s<sup>-1</sup>, respectively. The values of the consumption levels have been adapted from Yu & Cringle (2001) and Rahimy *et al.* (2015). All the other model parameter values and units are reported in Table 6. Additional details can be found in Chiaravalli (2018) and Verticchio Vercellin *et al.* (2021). Ultimately, we adopt the following piecewise constant definition of  $\mathcal{Q}^{\text{max}}(z)$  (units: mmHg/s):

$$Q^{\max}(z) = \begin{cases} 0 & z \in 0 \le z \le 15, \quad 55 \le z \le 145 \quad \mu \text{m}, \\ 90 & z \in 15 \le z \le 55 \,\mu \text{m}, \\ 26 & z \in 175 \le z \le 220, \quad 247 \le z \le 265, \quad 265 \le z \le 335 \quad \mu \text{m}, \\ 52 & z \in 145 \le z \le 175, \quad 220 \le z \le 247 \quad \mu \text{m}. \end{cases}$$

$$(4.6)$$

#### 4.4 Numerical approximation of the retinal oxygenation model

The computer simulation of the process of oxygen delivery and consumption in the retinal tissue comprises two steps:

1. linearization of the nonlinear reaction—diffusion problem (4.1) using a fixed-point iteration similar to that employed to solve the nonlinear algebraic system (3.19):

given  $p^{(0)} = p^{(0)}(z)$ ,  $z \in \overline{\Omega}_z$ , with  $p^{(0)}(0) = p_{\text{ch}}$ ,  $p^{(0)}(t_{rel}) = p_{\text{vit}}$  and  $p^{(0)}(z) > 0$  for all  $z \in \Omega_z$ , solve at each step l,  $l \ge 0$ , until convergence, the following linear reaction—diffusion boundary-value problem:

$$-D\alpha \frac{d^2 p^{(l+1)}(z)}{dz^2} + \sigma^{(l)} p^{(l+1)}(z) = g^{(l)} \quad \text{in } \Omega_z, \tag{4.7a}$$

$$p^{(l+1)}(0) = p_{\rm ch}, (4.7b)$$

$$p^{(l+1)}(t_{ret}) = p_{vit},$$
 (4.7c)

where  $\sigma^{(1)}$  and  $g^{(1)}$  are nonnegative functions depending on  $p^{(1)}$ ;

**2.** discretization of the sequence of linearized reaction-diffusion problems (4.7) using the finite element method.

The main properties of the algorithm for the approximation of the partial pressure of oxygen  $p_h = p_h(z)$  can be summarized as follows:

- 1. the number of iterations required by the fixed-point iteration procedure to satisfy the analog of the stopping criterion (3.24) markedly depends on the biophysical conditions characterizing the simulation test (see also Verticchio Vercellin *et al.*, 2021);
- 2. despite the piecewise definition of the reaction-diffusion model coefficients illustrated in Section 4.3,  $p_h$  is a continuous function for all  $z \in \overline{\Omega}_z$ ;
- 3.  $p_h(z) > 0$  for all  $z \in \overline{\Omega}_z$ .

More details on the construction and analysis of the fixed-point iteration and the related finite element approximation procedure described above can be found in Chiaravalli (2018), Causin *et al.* (2016) and Verticchio Vercellin *et al.* (2021).

#### 5. Results

In this section, the multi-scale/multi-physics model outlined in Sections 3 and 4 is used to simulate the impact of two pathological conditions, namely IOP elevation and CRVO, on the hemodynamics and oxygenation of the retina under the assumptions that the three capillary plexuses SCP, ICP and DCP are connected either *in series* or *in parallel*. Ultimately, the goal is to provide quantitative insights into which capillary architecture is the more plausible when compared to the outcomes observed experimentally.

To help identify and characterize differences in the hemodynamic responses to IOP elevation and CRVO as the *in series* or *in parallel* configurations are considered, we introduce two specific quantities of interest. In the *in series* case, the capillary plexuses experience the same flow Q but different pressure drops  $\Delta P_i$  and different average pressures  $\hat{P}_i$ , so that we can define the percent variation of the pressure  $\hat{P}_i$  experienced by the plexus  $i \in \mathcal{C}$  as

$$\delta(\hat{P}_i^*) = \frac{\hat{P}_i^* - \overline{\hat{P}_i^*}}{\overline{\hat{P}_i^*}} \cdot 100 \quad i \in \mathcal{C}, \tag{5.1}$$

where  $\overline{\hat{P}_i^*}$  and  $\hat{P}_i^*$  represent the average pressure in the plexus i in the reference and altered conditions, respectively. In the *in parallel* case, the capillary plexuses experience the same

pressure drop  $\Delta P$  but different flow rates  $Q_i$ , so that we can define the percent variation of the flow rate  $\delta(Q_i)$  experienced by the plexus  $i = \mathcal{C}$  as

$$\delta(Q_i^*) = \frac{Q_i^* - \overline{Q_i^*}}{\overline{Q_i^*}} \cdot 100 \quad i \in \mathcal{C}, \tag{5.2}$$

where  $\overline{Q_i^*}$  and  $Q_i^*$  represent the flow rate in the plexus i in the reference and altered conditions, respectively.

#### 5.1 IOP elevation

The effect of IOP elevation is simulated by increasing the external pressure  $p_{\rm ext}$  acting on the retinal vessels from a reference value of 15 mmHg up to a value of 42.5 mmHg. Fig. 8 shows the average pressure  $\hat{P}_i^*$  and the blood flow  $Q_i^*$  in the three capillary plexuses in the *in series* and *in parallel* configurations, respectively. In both configurations, significant changes with respect to the reference condition occur when IOP reaches the value of 25 mmHg. In the *in series* configuration, the pressure experienced by the three capillary plexuses starts to increase, approaching a plateau value of about 50 mmHg. We note that a pressure value of 50 mmHg is quite elevated for a capillary and is more compatible with the pressure in a larger vessel such as the CRA. The highest value of the pressure is attained by the SCP. In *the parallel* configuration, the blood flow streaming across the three capillary plexuses decreases in all three compartments, attaining the smallest values in the DCP.

Fig. 9 illustrates the percent changes in pressure  $\delta(\hat{P}_i^*)$  and volumetric flow rate  $\delta(Q_i^*)$  predicted by the model in each capillary plexus for the *in series* and *in parallel* configurations, respectively, as increments in IOP, denoted by  $\Delta$ IOP, are considered between 5 and 25 mmHg with respect to the reference IOP value of 15 mmHg. In the *in series* configuration, as shown also by Fig. 8, the pressure in the capillaries increases with higher IOP and this increase is not uniform among the three capillary plexuses. The percent variation of pressure among them appears to be higher at the DCP and ICP level with respect to the SCP, particularly when  $\Delta$ IOP is larger than 15 mmHg. As IOP increases, the variation among the three capillary plexuses becomes more significant, reaching a difference of about 15% between the DCP and the ICP when  $\Delta$ IOP = 25 mmHg. In the *in parallel* configuration, all the three capillary plexuses seem to exhibit a similar decrease in flow as a consequence of the increased vascular resistance resulting from the IOP-induced vessel compression.

Fig. 10 shows the spatial distribution of partial pressure of oxygen *p* across the retinal thickness for IOP equal to the reference value of 15 mmHg and at the elevated values of 25 and 35 mmHg, respectively. Comparing the reference situation curve (IOP = 15 mmHg) between the two capillary configuration (Fig. 10, left and right), a major difference can be seen in the value of the partial pressure of oxygen in the ONL. In the *in series* configuration, the *p* values in the ONL are around 10 mmHg, which is more than two times the values predicted in the same region when the *in parallel* configuration is considered. Interestingly, in the *in series* configuration the IOP elevation causes a significant decrease in the partial pressure of oxygen mainly in the central layers of the retina, namely in the ONL, OPL and INL. These layers, indeed, are those proximal to the DCP and ICP, which according to

vascular model predictions are the most affected by IOP elevation. Conversely, the effects in correspondence of the SCP layers appear to be negligible. In the *in parallel* configuration, IOP elevation causes a significant decrease in *p* in the proximity of all the three plexuses, both in the central retina ONL, OPL and INL, and in the layer next to the vitreous, namely the GCL.

#### 5.2 Central retinal vein occlusion

The CRVO is simulated by reducing the value of the radius of the CRV by different percentages in the Starling formula (3.16). This corresponds to modifying the value of  $A_{\rm ref}$  in Eq. (3.16). Reductions of  $A_{\rm ref}$  ranging between 10% and 80% have been considered. Fig. 11 shows the average pressure  $\hat{P}^*$  and the blood flow  $Q^*$  across the three capillary plexuses when reducing the radius of the CRV in the model. As CRVO becomes more severe, the system is able to respond by maintaining an almost constant pressure (*in series*) and blood flow (*in parallel*) up to an occlusion of the vessel equal to 60%. Above this value, the pressure in the capillaries in the *in series* configuration increases, reaching the value of 50 mmHg in correspondence of an occlusion of 80%: in this condition the three capillary plexuses almost attain the same internal pressure. In the parallel configuration, above a CRVO of 60%, we observe a reduction of the blood flow in all the three plexuses.

Fig. 12 illustrates the percent changes in pressure drops  $\delta(\hat{P}^*)$  and volumetric flow rate  $\delta(Q^*)$  for the *in series* and *in parallel* configurations, respectively, as various degrees of CRVO % are considered. Similarly to the case of IOP elevation, increasing CRVO % in the *in series* configuration, the DCP and the ICP seem to exhibit higher percent variations with respect to the SCP. A significant increase of the pressure (>20%) occurs, coherently with Fig. 11 (left panel), for an occlusion of the vessel equal to 70%. When CRVO reaches 80%, the pressure inside the DCP is more than doubled with respect to the reference value. Unlike the *in series* configuration, in the *in parallel* configuration the three capillary plexuses show a uniform percent variation of the blood flow across each of them, the most relevant variations in the blood flow (>20%) occurring for a CRVO of 70%. Results shown in Fig. 11 (and Fig. 12) indicate a sudden increase (decrease) in the hemodynamic response of the retinal vasculature as a function of the level of occlusion of CRV. This common sudden trend may be ascribed to the nonlinear dependence of the resistance of CRV, CRA and venules on the transmural pressure difference as modelled in Eq. (3.16). Until a certain level of occlusion (corresponding to a certain level of reduction of the vessel cross-section area  $A_{ref}$ ), both in series and in parallel configurations seem to be able to compensate for the occlusion, so that the average pressure and blood flow remain unchanged. Once a limit level of occlusion is reached, the vascular resistance increases so significantly that the average pressure in SCP, DCP and ICP becomes suddenly higher (in the in series configuration) and, correspondingly, the blood flow becomes suddenly smaller (in the *in parallel* configuration). Unlike the case of *in series* configuration, in the *in parallel* configuration the blood flow in the three layers with a CRVO of 80% undergoes a uniform percent variation of around 75%.

Fig. 13 illustrates the spatial distribution of partial pressure of oxygen *p* across the retinal thickness in the absence of CRVO and at 20%, 50% and 80% levels of occlusion. A comparison between the left and right panels in Fig. 13 suggests that the *in parallel* 

configuration is less affected by an impairment of 20–50%, while in the *in series* configuration the variation appears more relevant. When CRVO reaches 80% the partial pressure of oxygen in the central part of the retina becomes minimum in both vascular configurations. The GCL layer instead is affected only considering a parallel arrangement of the microvascular structure. Consistently with model predictions in the case of IOP elevation, in the *in series* configuration, the most affected layers are those proximal to the DCP and the ICP, ONL, OPL and INL, while almost no effect is visible on the GCL, supplied by the SCP. In *the parallel* configuration, instead, also the GCL is affected. Consistent with Fig. 12 (right) all the capillary plexuses appear to be affected in a uniform manner.

#### 6. Discussion

The results illustrated in Section 5 provide a quantitative way to interpret clinical data and allow us to infer which between the *in series* and *in parallel* configurations is more consistent with the clinical observations. Overall, the model predictions can be summarized as follows:

- show that the three capillary plexuses respond in a uniform way to IOP elevation and increasing CRVO. From the oxygen profiles in the right panels of Figs. 10 and 13 it appears that the inner region of the retina, in particular the GCL, INL and OPL, is the most impacted by both IOP elevation and increasing CRVO.
- In series configuration: the histograms in the left panels of Figs. 9 and 12 show that the three capillary plexuses respond differently to IOP elevation and increasing CRVO. In particular, the ICP and the DCP appear to be more affected than the superficial plexus. This behaviour is also reflected in the oxygen profiles reported in the left panels of Figs. 10, where the layers that appear to be more affected by lack of oxygen are those surrounding these vascular layers, in particular in the central region of the retina, involving the INL, the OPL and the ONL.

#### 6.1 IOP elevation

The results reported in Fig. 9 suggest that the three plexuses in the *in series* case are affected by the increase of IOP in a different way, with a stronger impact on DCP and ICP compared to SCP. Conversely, in the *in parallel* configuration, the volumetric blood flow percentage variation as IOP increases in the three capillary plexuses is uniform: the three vascular layers suffer in the same way the increasing IOP, suggesting that a pathological increase in IOP would affect the three capillary plexuses in the same way. In a clinical study performed on rats (Bui *et al.*, 2018), the authors tested the behaviour of the three capillary plexuses to IOP elevation. They found that the two deepest capillary plexuses in the rat retina, the intermediate and deep vascular plexuses, have a greater capacity to respond to changes in IOP with respect to the superficial capillary plexuses. As reported in Bui *et al.* (2018), this may suggest a redistribution of the blood towards the deepest layers of the retina in the

case of IOP elevation. These results are consistent with the *in series* configuration, which reported a differential response of the three layers to IOP elevation.

#### 6.2 Central retinal vein occlusion

The results reported in Fig. 12 suggest that the three plexuses in the *in series* case are affected by a CRVO of increasing severity in a different way, with a stronger impact on DCP and ICP compared to SCP. Conversely, in the in parallel configuration, the volumetric blood flow percentage variation as CRVO increases in the three capillary plexuses is uniform: the three vascular layers suffer in the same way the increasing CRVO, suggesting that a pathological increase in CRVO would affect the three capillary plexuses in the same way. In the in series configuration, SCP is slightly affected by the vein occlusion whereas DCP experiences a stronger variation in pressure, consistent with data from the literature (Ghasemi et al., 2017; Rahimy et al., 2015; Sarraf et al., 2013). Moreover, in the in series configuration the venous drainage of the capillaries is totally deputed to the DCP, the only plexus in direct contact with the vein district in the model, which as a consequence turns out to be the most affected by an increase of CRVO. This hypothesis, which seems to favour the *in series* configuration, seems also to be consistent with clinical data concerning PAMM, a pathology secondary to CRVO. PAMM is mainly attributed to ischemia of DCP, in accordance with data supporting the hypothesis that DCP is the main plexus devoted to the venous drainage of the vascular system (Garrity et al., 2017; Paques et al., 2003) and, sometimes, also of the ICP (Rahimy et al., 2015; Sarraf et al., 2013). These conjectures are consistent with the in series configuration, which reported a differential response of the three layers to an increase of CRVO.

#### 6.3 Model limitations and improvement

The theoretical model proposed in the present work is affected by two main limitations:

The first limitation concerns with the capillary distribution inside each capillary plexus, which is mathematically described by formula (3.3). Such description is driven by the information available in Campbell *et al.* (2017), which solely consists of the value of the capillary density  $\gamma_i$ ,  $i = \mathcal{C}$ . Should a richer information on the geometrical properties of the capillary network be available, then, it could be profitably employed to improve the accuracy in the evaluation of  $R_{eq,i}$ ,  $i = \mathcal{C}$ . This is expected to quantitatively modify model predictions without changing significantly their qualitative behaviour and which of the two configurations (in series or in parallel) is more physiologically plausible.

The second limitation concerns with the choice of the values of the thickness of each layer in Fig. 7, which are chosen in the present work consistent with available data for the parafoveal region (Terry *et al.*, 2016). The study of a different anatomical region of the retina would require the use of a different set of values for the retinal layer thicknesses. A special treatment is in order when dealing with the macular region, which is characterized by a marked nonuniformity of the layer thicknesses.

## 7. Conclusions and future perspectives

The proposed multi-scale/multi-physics mathematical model allowed us to simulate two possible vascular configurations of the retinal capillary plexuses, testing them under IOP elevation and CRVO. The results, consistent with clinical data (Bui et al., 2018; Ghasemi et al., 2017; Rahimy et al., 2015; Sarraf et al., 2013), seem to suggest that the in series configuration better describes the physiology of the retinal capillary network in health and disease. Mathematical modelling has allowed us to study a complex system in different simulated scenarios and has led to a possible interpretation of newly available experimental data. With the availability of new and more accurate data, new studies may also involve other regions of the retina, for example taking into account the interconnection of the radial peripapillary capillary plexuses with the other layers, which may have an important role in the vascularization and oxygenation of the peripheral retina. The availability of more detailed and quantitative information on the length and diameter of the single capillaries could also lead to a more accurate estimate of the resistance of each vascular layer. While the present study was performed by simulating the conditions of IOP elevation and CRVO because of the availability of clinical data, its conclusions are broadly applicable. New insights into retinal capillary organization gained from this model should contribute to the understanding of normal retinal physiology as well as to a variety of pathophysiological states, as most eye diseases have a hemodynamic component. Conclusions regarding the in series arrangement of retinal capillaries may be of particular interest to those seeking to further understand ischemic optic neuropathy, retinal artery occlusion, hypertensive retinopathy, glaucoma and diseases of retinal neovascularization including macular degeneration, diabetic retinopathy and retinopathy of prematurity. As the medical community's understanding of retinal capillary organization and flow dynamics continues to grow, further insight will be gained into the pathophysiology of retinal ischemia. Such insight may prove key in the future development of novel approaches in the treatment of severe retinal pathologies such as central and branch retinal vein occlusions as well as paracentral acute middle maculopathy.

## **Funding**

This work was supported by NIH grant R01EY030851 (A.H.), NSF DMS 1853222/2021192 (G.G. and A.H.) and a Challenge Grant award from Research to Prevent Blindness, NY (A.H.).

#### References

- Arciero JC, Carlson BE & Secomb TW (2008) Theoretical model of metabolic blood flow regulation: roles of ATP release by red blood cells and conducted responses. Amer. J. Physiol. Heart Circ. Physiol, 295, H1562–H1571. [PubMed: 18689501]
- Arciero J, Harris A, Siesky B, Amireskandari A, Gershuny V, Pickrell A & Guidoboni G (2013) Theoretical analysis of vascular regulatory mechanisms contributing to retinal blood flow autoregulation. Invest. Ophthalmol. Vis. Sci, 54, 5584–5593. [PubMed: 23847315]
- Bui BV, Zhao D, Wang L, Fortune B & He Z (2018) Response of the trilaminar retinal vessel network to intraocular pressure elevation in rat eyes. Invest. Ophthalmol. Vis. Sci, 61, 2.
- Cabral D, Pereira T, Ledesma-Gil G, Rodrigues C, Coscas F, Sarraf D, Freund KB (2020) Volume rendering of dense B-scan optical coherence tomography angiography to evaluate the connectivity of macular blood flow.Invest. Ophthalmol. Vis. Sci, 61, 44.

Campbell JP, Zhang M, Hwang TS, Bailey ST, Wilson DJ, Jia Y & Huang D (2017) Detailed vascular anatomy of the human retina by projection-resolved optical coherence tomography angiography. Sci. Rep, 7, 1–11. [PubMed: 28127051]

- Causin P, Guidoboni G, Malgaroli F, Sacco R & Harris A (2016) Blood flow mechanics and oxygen transport and delivery in the retinal microcirculation: multiscale mathematical modeling and numerical simulation. Biomech. Model. Mechanobiol, 15, 525–542. [PubMed: 26232093]
- Chandrasekera E, An D, McAllister IL, Yu D & Balaratnasingam C (2018) Three-dimensional microscopy demonstrates series and parallel organization of human peripapillary capillary plexuses. Invest. Ophthalmol. Vis. Sci, 59, 4327–4344. [PubMed: 30193305]
- Chiaravalli G (2018) A virtual laboratory for retinal physiology: a theoretical study of retinal oxygenation in healthy and disease. Master thesis, Politecnicno di Milano.
- Fouquet S, Vacca O, Sennlaub F & Paques M (2017) The 3D retinal capillary circulation in pigs reveals a predominant serial organization. Invest. Ophthalmol. Vis. Sci, 58, 5754–5763. [PubMed: 29114842]
- Freund KB, Sarraf D, Leong BCS, Garrity ST, Vupparaboina KK & Dansingani KK (2018)
  Association of optical coherence tomography angiography of collaterals in retinal vein occlusion with major venous outflow through the deep vascular complex. JAMA Ophthalmol, 136, 11.
- Ganfield RA, Nair P & Whalen WJ (1970) Mass transfer, storage, and utilization of O2 in cat cerebral cortex. Am. J. Physiol, 219, 814. [PubMed: 5450892]
- Garrity ST, Paques M, Gaudric A, Freund KB & Sarraf D (2017) Considerations in the understanding of venous outflow in the retinal capillary plexus. Retina, 37, 1809–1812. [PubMed: 28737534]
- Ghasemi FK, Phasukkijwatana N, Freund KB, Cunningham ET, Kalevar A, McDonald HR, Dolz-Marco R, Roberts PK, Tsui I, Rosen R, Jampol LM, Sadda SR & Sarraf D (2017) En face optical coherence tomography analysis to assess the spectrum of perivenular ischemia and paracentral acute middle maculopathy in retinal vein occlusion. Am. J. Ophthalmol, 177, 131–138. [PubMed: 28237415]
- Goldenberg D, Shahar J, Loewenstein A, Goldstein M (2013) Diameters of retinal blood vessels in a healthy cohort as measured by spectral domain optical coherence tomography. Retina, 33, 1888–1894. [PubMed: 23719399]
- Guidoboni G, Harris A, Carichino L, Arieli Y & Siesky BA (2014a) Effect of intraocular pressure on the hemodynamics of the central retinal artery: a mathaematical model. Math. Biosci. Eng, 11, 523–546. [PubMed: 24506550]
- Guidoboni G, Harris A, Cassani S, Arciero J, Siesky B, Amireskandari A, Tobe L, Egan P, Januleviciene I & Park J (2014b) Intraocular pressure, blood pressure, and retinal blood flow autoregulation: A mathematical model to clarify their relationship and clinical relevance. Invest. Ophthalmol. Vis. Sci, 55, 4105–4118. [PubMed: 24876284]
- Lavia C, Mecê P, Nassisi M, Bonnin S, Marie-Louise J, Couturier A, Erginay A, Tadayoni R & Gaudric A (2020) Retinal capillary plexus pattern and density from fovea to periphery measured in healthy eyes with swept-source optical coherence tomography angiography. Sci. Rep, 10, 1474. [PubMed: 32001769]
- Linsenmeier RA & Braun RD (1992) Oxygen distribution and consumption in the cat retina during normoxia and hypoxemia. J. Gen. Physiol, 99, 177–197. [PubMed: 1613482]
- Paques M, Tadayoni R, Sercombe R, Laurent P, Genevois O, Gaudric A & Vicaut E (2003) Structural and hemodynamic analysis of the mouse retinal microcirculation. Invest. Ophthalmol. Vis. Sci, 44, 4960–4967. [PubMed: 14578423]
- Pogue BW, O'Hara JA, Wilmot CM, Paulsen KD & Swartz HM (2001) Estimation of oxygen distribution in RIF-1 tumors by diffusion model-based interpretation of pimonidazole hypoxia and eppendorf measurements. Radiat. Res, 155, 15–25. [PubMed: 11121211]
- Quarteroni A, Sacco R & Saleri F (2007) Numerical Mathematics, Second Edition. Numerical Mathematics, vol. 37. New York: Springer.
- Rahimy E, Kuehlewein L, Sadda SR & Sarraf D (2015) Paracentral acute middle maculopathy. Retina, 35, 1921–1930. [PubMed: 26360227]
- Sacco R, Guidoboni G & Mauri A (2019) A Comprehensive Physically Based Approach to Modeling in Bioengineering and Life Sciences, Ch. 15, 1st edn. Elsevier, Academic press.

Sarraf D, Rahimy E, Fawzi AA, Sohn E, Barbazetto I, Zacks DN, Mittra RA, Klancnik JM, Mrejen S, Goldberg NR, Beardsley R, Sorenson JA, Freund KB (2013) Paracentral acute middle maculopathy. JAMA Ophthalmol, 131, 1275–1287 10 [PubMed: 23929382]

- Scharf J, Freund KB, Sadda S & Sarraf D (2018) Paracentral acute middle maculopathy and the organization of the retinal capillary plexuses. Prog. Retin. Eye Res, 81, 100884.
- Terry L, Cassels N, Lu K, Acton JH, Margrain TH, North RV, Fergusson J, White N & Wood A (2016) Automated retinal layer segmentation using spectral domain optical coherence tomography: evaluation of inter-session repeatability and agreement between devices. PLoS One, 11, 1–15.
- Yu DY & Cringle SJ (2001) Oxygen distribution and consumption within the retina in vascularised and avascular retinas and in animal models of retinal disease. Prog. Retin. Eye Res, 20, 175–208. [PubMed: 11173251]
- Yu D, Cringle SJ, Yu PK, Balaratnasingam C, Mehnert A, Sarunic MV, An D & Su E (2019) Retinal capillary perfusion: spatial and temporal heterogeneity. Prog. Retin. Eye Res, 70, 23–54. [PubMed: 30769149]
- Verticchio Vercellin AC, Harris A, Chiaravalli G, Sacco R, Siesky B, Ciulla T & Guidoboni G (2021) Physics-based modeling of age-related macular degeneration a theoretical approach to quantify retinal and choroidal contributions to macular oxygenation. Math. Biosci, 339, 108650. [PubMed: 34197878]

## IN PARALLEL

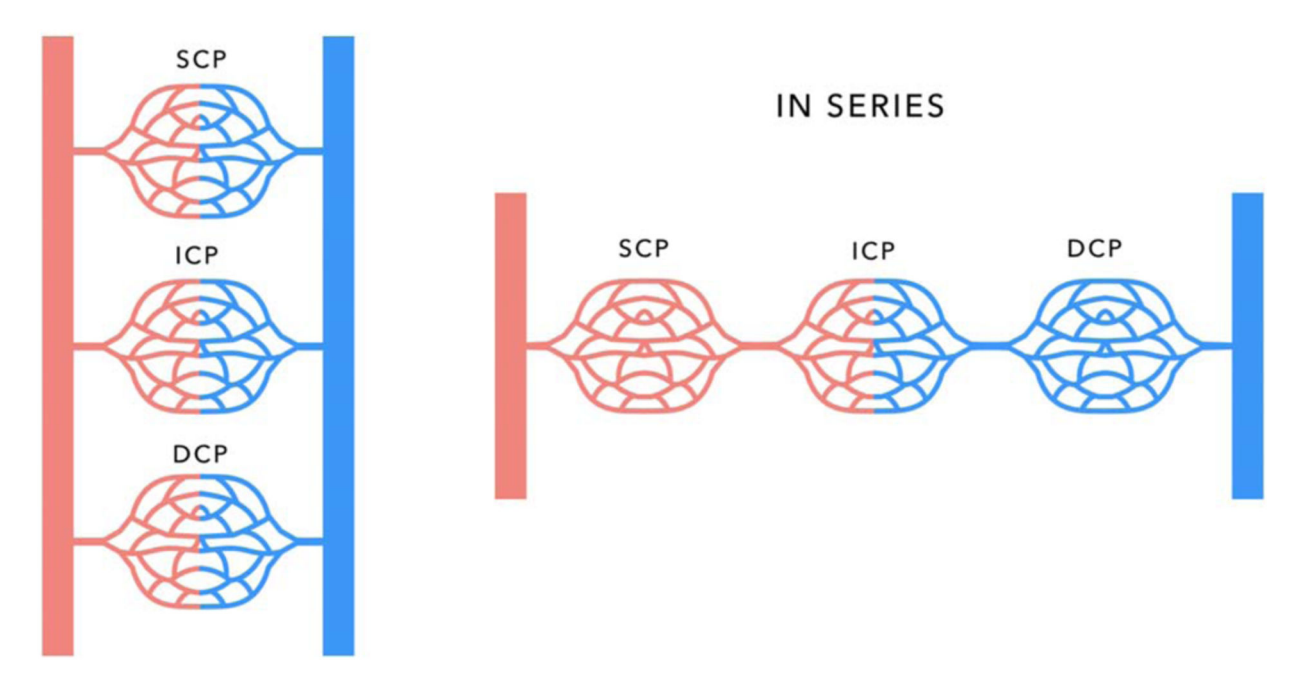
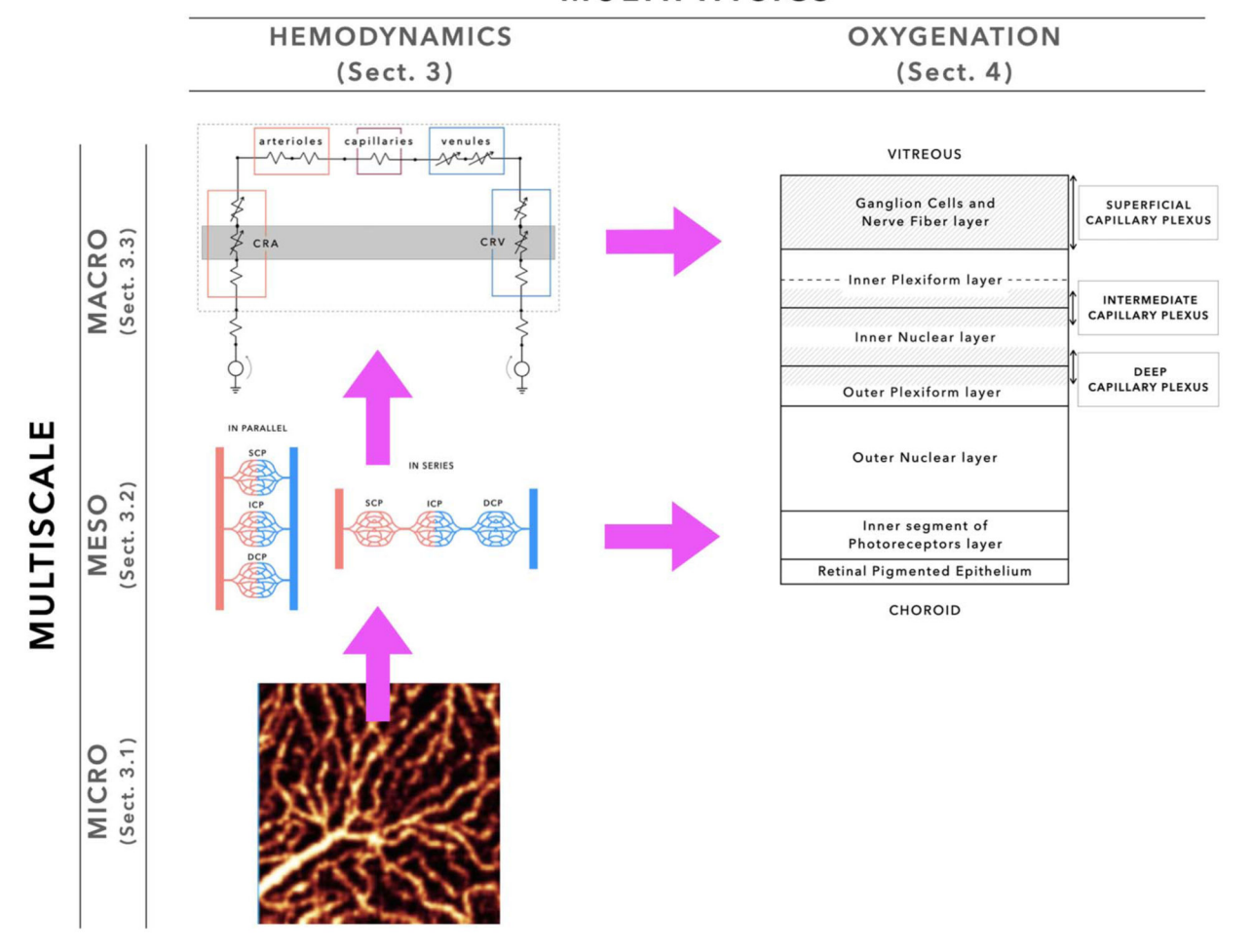


Fig. 1. Schematic representation of the two hypothesized vascular configurations: on the left, the plexuses are connected *in parallel*, on the right, they are connected *in series*. Each of the two configurations can be regarded as a micro-scale representation of retinal circulation.

## **MULTIPHYSICS**



**Fig. 2.** Schematic representation of the multi-scale/multi-physics modelling approach to retina physiology proposed in this article.

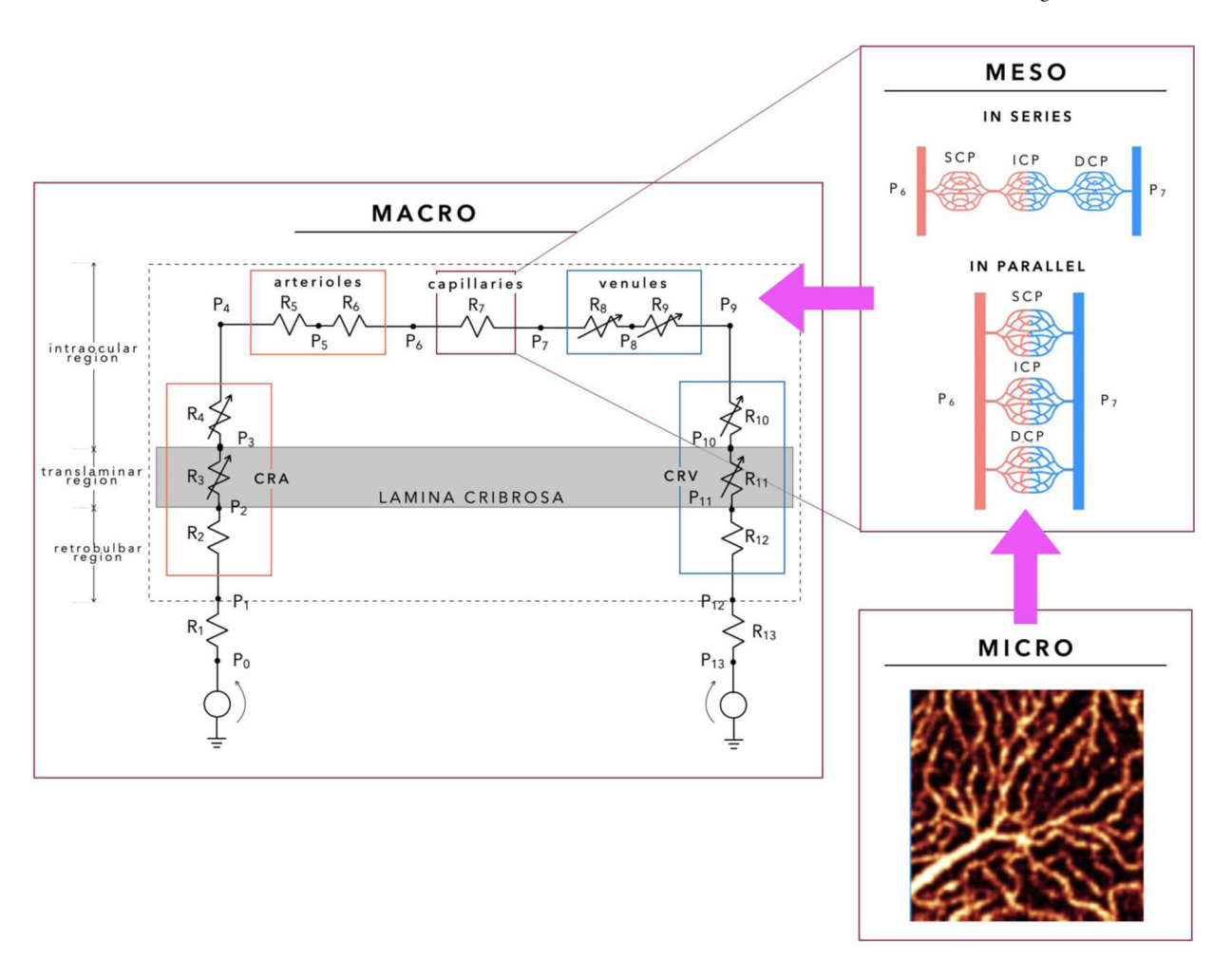


Fig. 3. Multi-scale representation of retinal hemodynamics. The circuit representation is based on the electric analogy to fluid flow and is a modified version of the model proposed in Guidoboni *et al.* (2014b). The scheme can be regarded as a macro-scale representation of retinal circulation. The zoomed panel shows the two vascular configurations considered for the capillary plexuses, namely *in series* and *in parallel*, and their representations at the meso-and micro- levels.

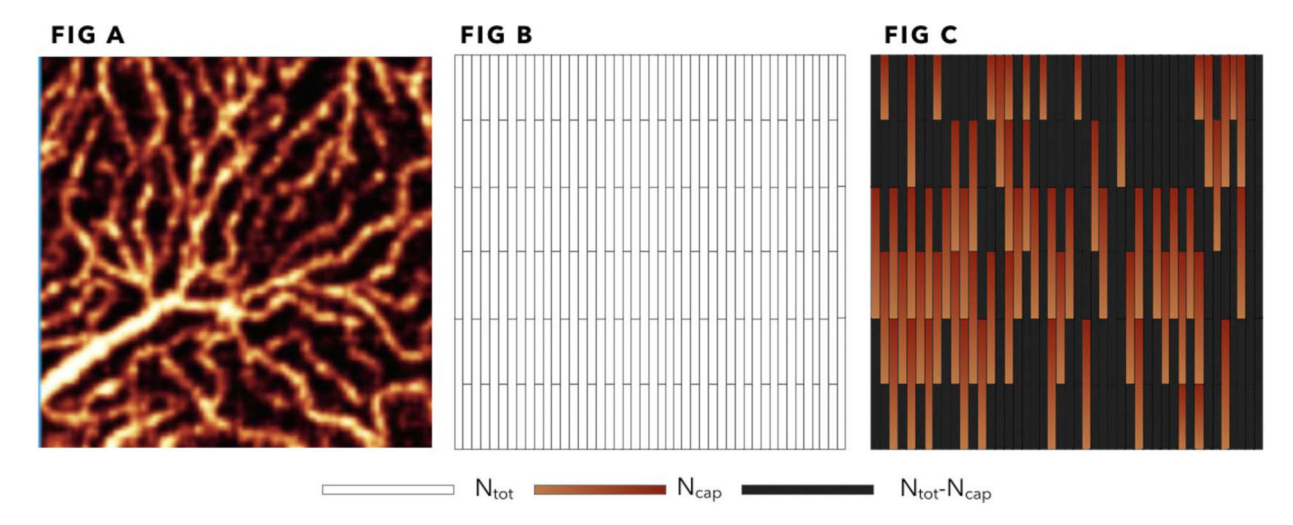
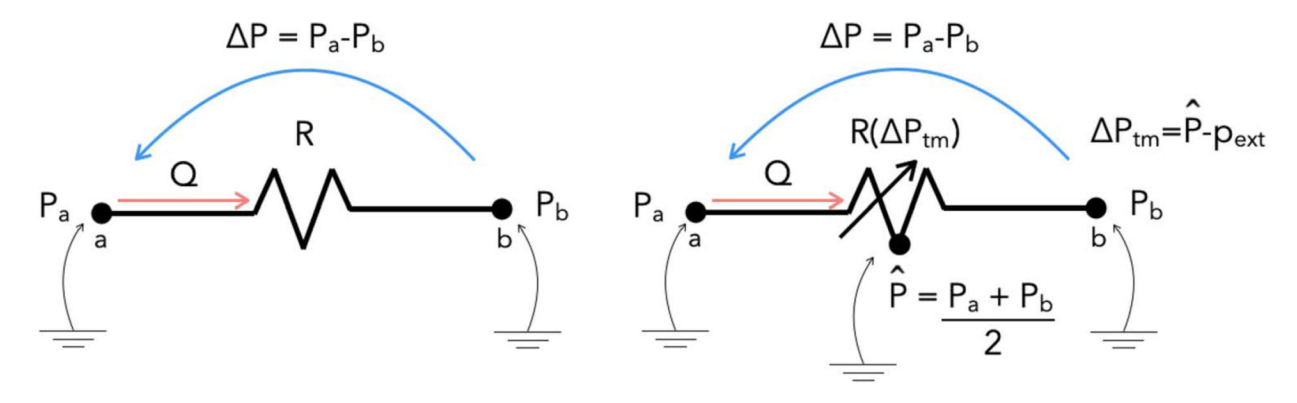
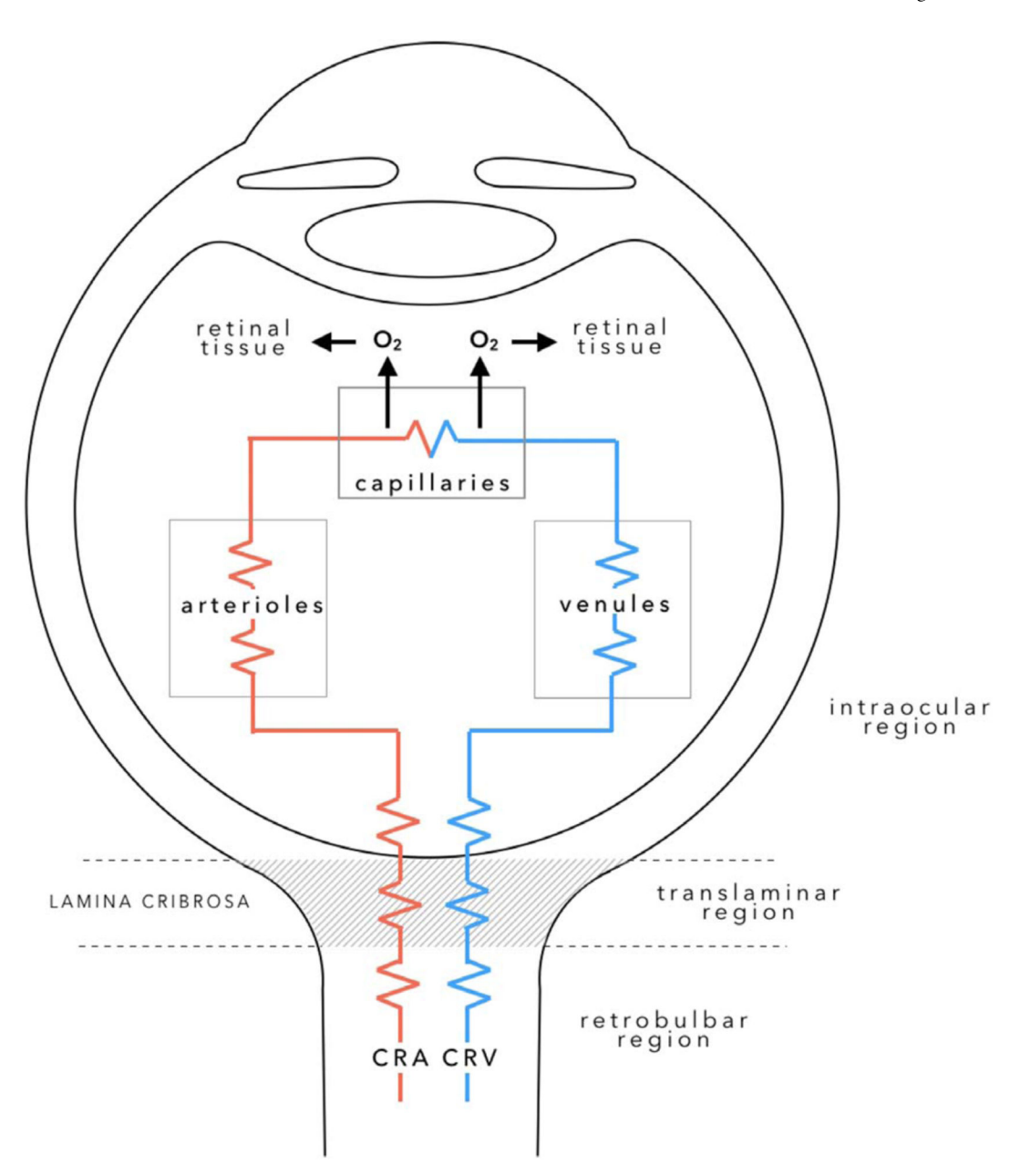


Fig. 4. (A) is taken from Campbell *et al.* (2017) and represents a typical image of a capillary plexus. (B) represents the subdivision of the total area of the image into  $N_{\text{tot}}$  rectangles. (C) shows a possible configuration in which  $N_{\text{cap,i}}$  rectangles are drawn in brown-red colour because each of them is occupied by a capillary, whereas the remaining  $N_{tot} - N_{\text{cap,i}}$  rectangles are drawn in black colour because they are not occupied by capillaries.



**Fig. 5.** Schematic representation of a linear resistor (left) and nonlinear resistor (right).



**Fig. 6.** Schematic representation of retinal circulation and the process of oxygen delivery. In this equivalent electric representation, oxygen delivery is modelled as an oxygen source localized at the level of the capillary district (black arrows in the figure).

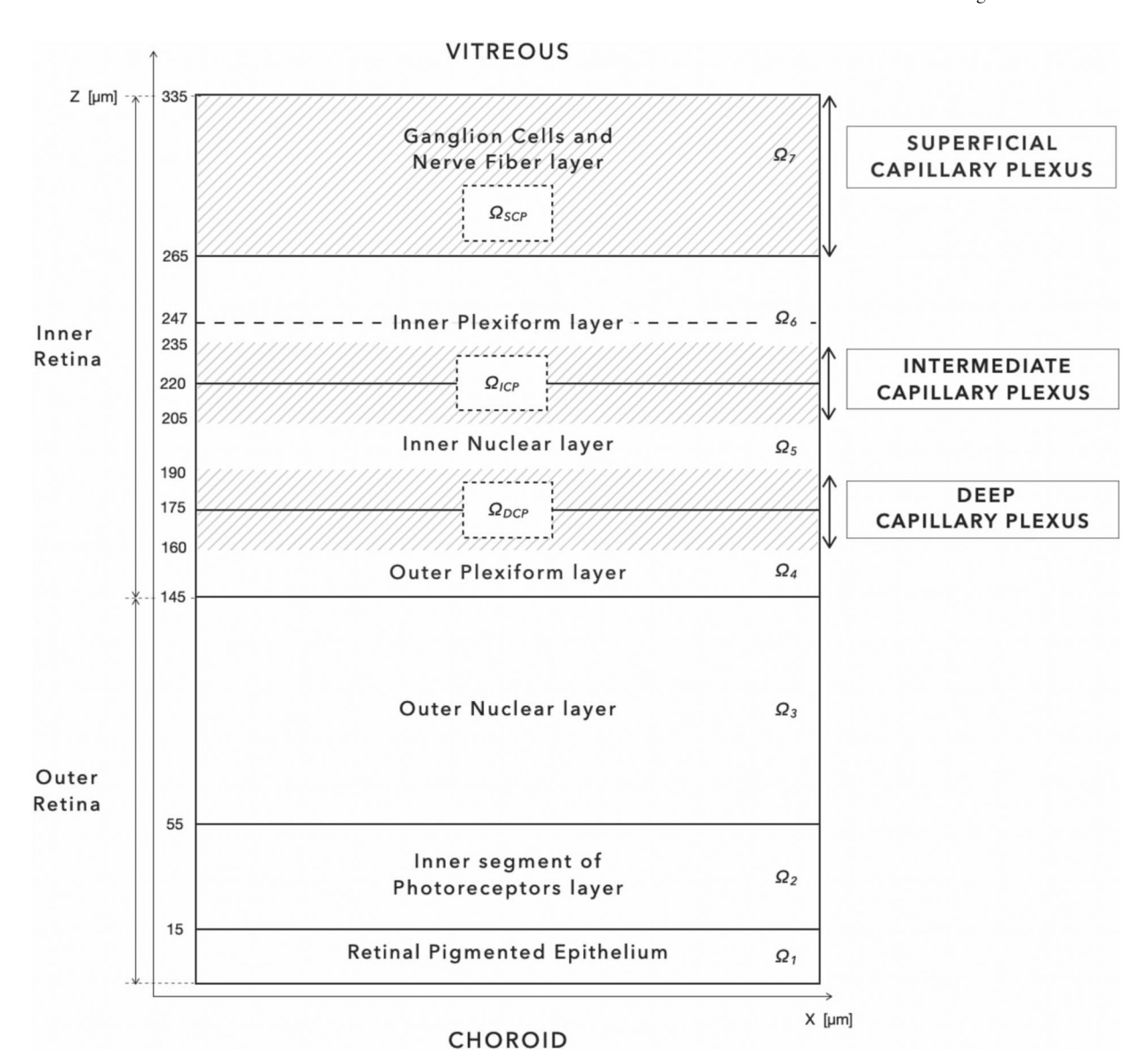


Fig. 7. Schematic representation of the different anatomical layers composing the retinal tissue. The shadowed areas represent the locations of the capillary plexuses. The coordinates of each layer are reported on the *z*-axis (units: \( \rho m \)).

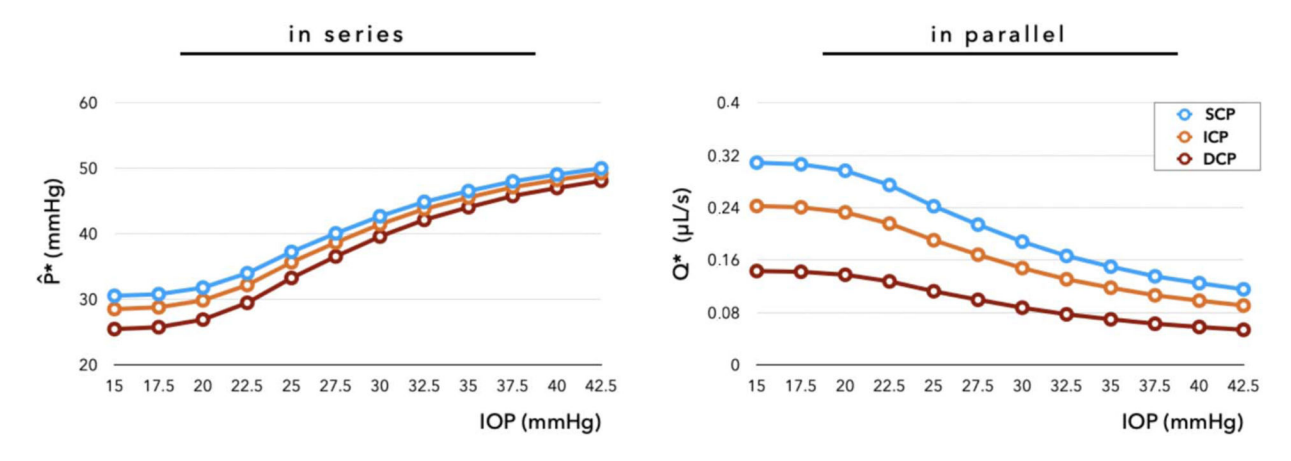


Fig. 8.  $\hat{P}_i^*$  and  $Q_i^*$  in the three capillary plexuses as a function of IOP.

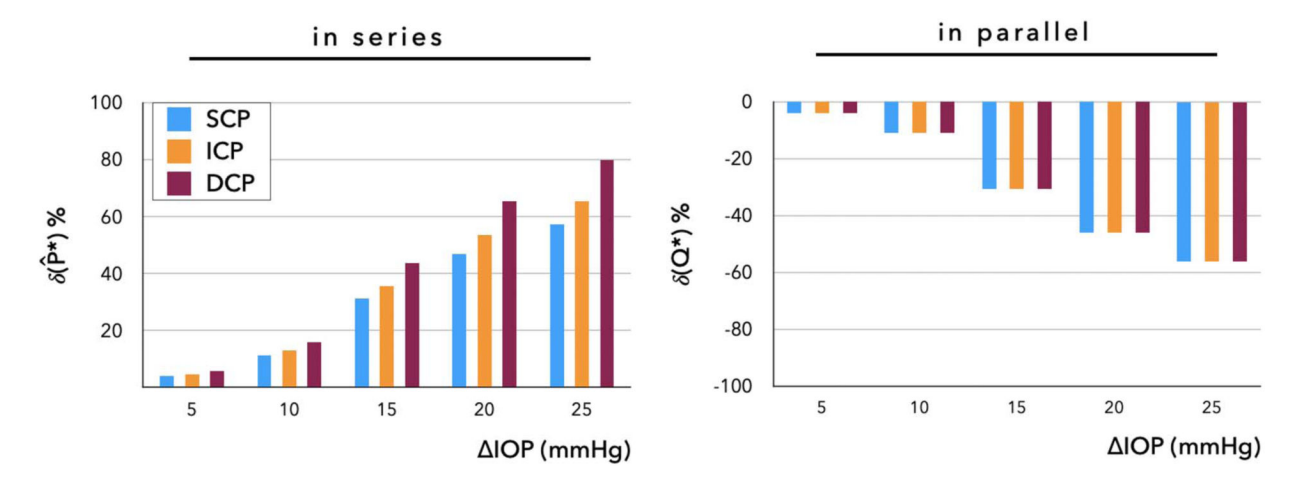
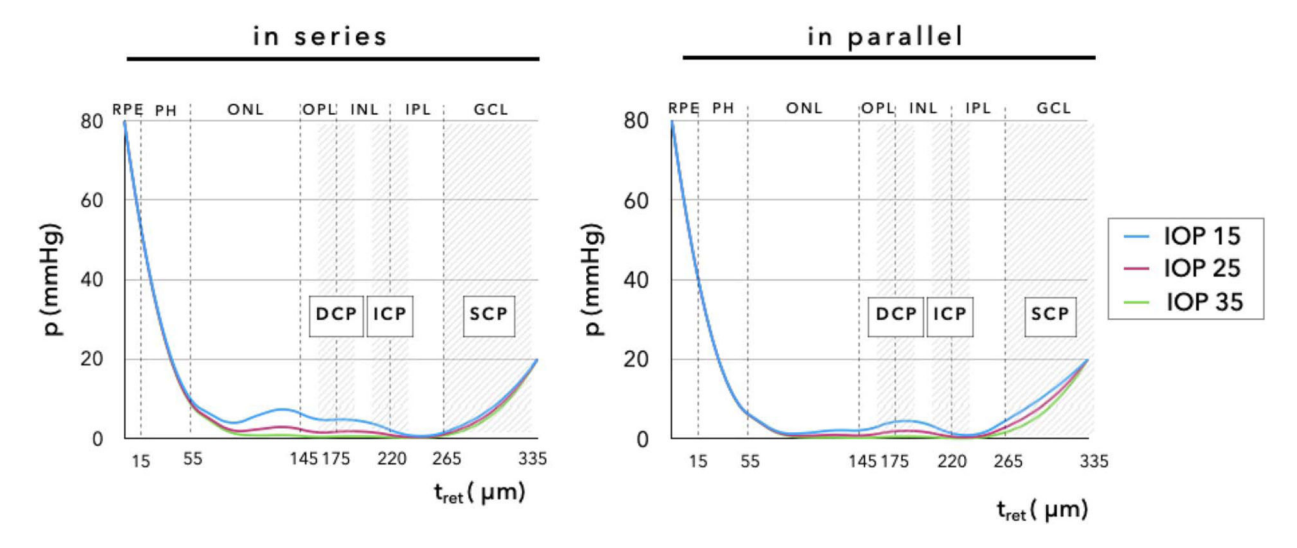


Fig. 9. Percent changes in pressure drops  $\delta(\hat{P}^*)$  and volumetric flow rate  $\delta(Q^*)$  are reported for the *in series* and *in parallel* configurations, respectively, as various increments  $\Delta$ IOP with respect to the reference IOP value are considered.



**Fig. 10.** Spatial distribution of partial pressure of oxygen *p* across the retinal thickness in the case where IOP is equal to the reference value of 15 mmHg and at the elevated values of 25 and 35 mmHg, respectively.

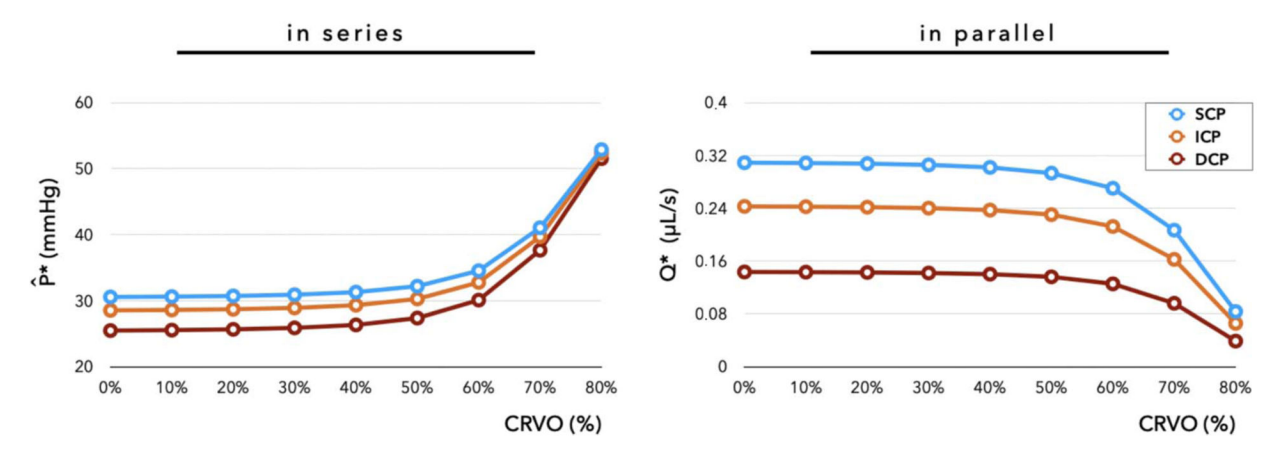


Fig. 11.  $\hat{P}_i^*$  and  $Q_i^*$  in the three capillary plexuses as a function of the elevating CRVO %.

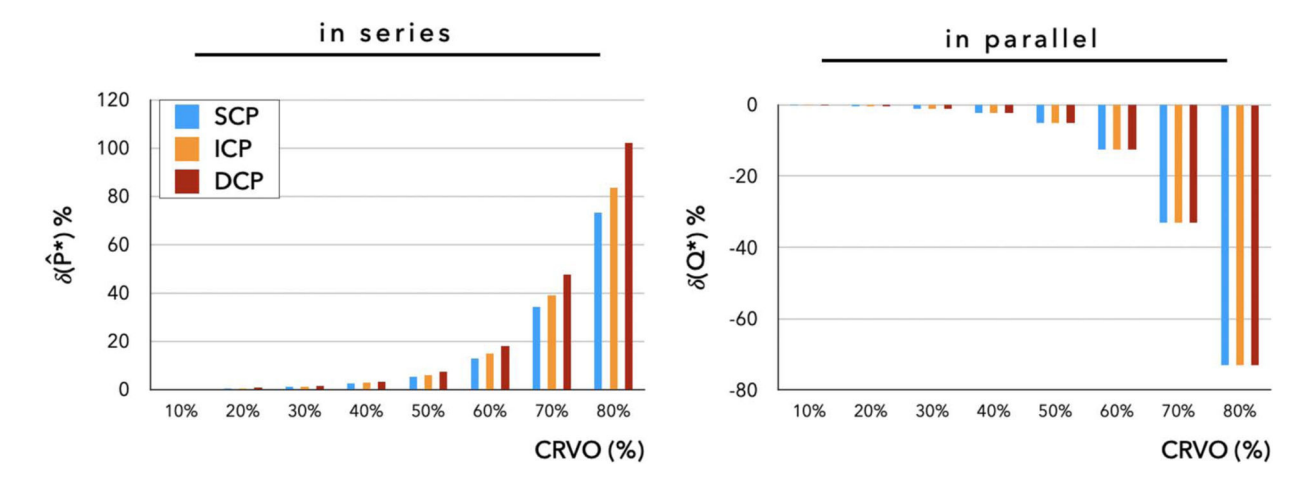


Fig. 12. Percent changes in pressure drops  $\delta(\Delta P)$  and volumetric flow rate  $\delta(Q)$  are reported for the *in series* and *in parallel* configurations, respectively, as various increasing levels of CRVO are considered.

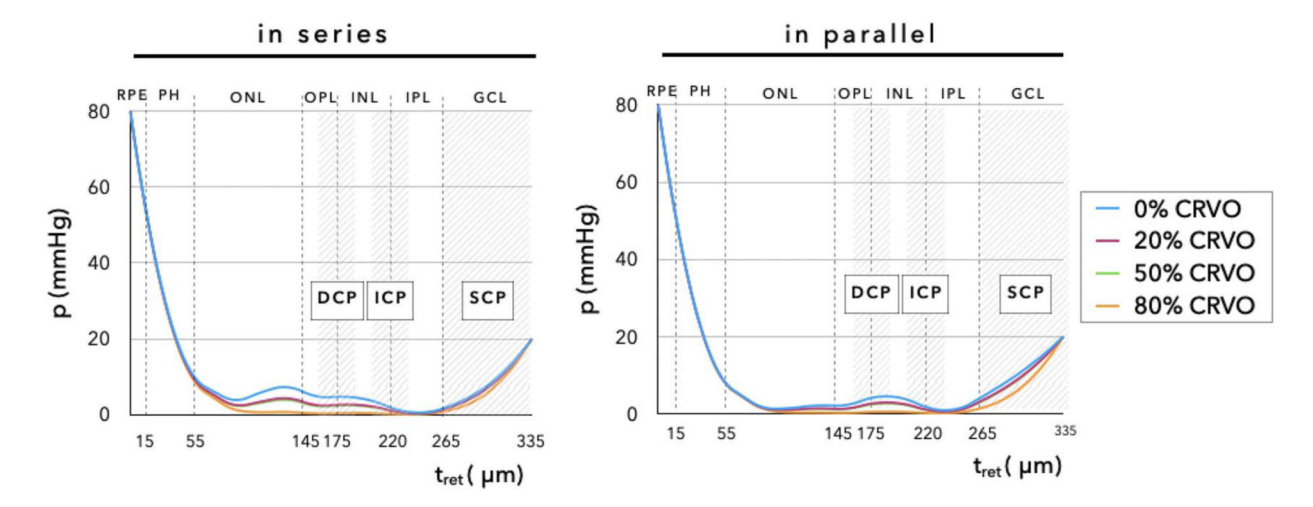


Fig. 13. Distributions of partial pressure of oxygen p across the retinal thickness in the absence of CRVO and at 20%, 50% and 80% levels of occlusion.

Table 1

Values of the vascular resistances in the reference configuration taken from Guidoboni et al. (2014b).

Resistance	Value	Resistance	Value
	$[mmHg \cdot s/mL]$		$[mmHg \cdot s/mL]$
$\overline{R}_1$	$2.25 \cdot 10^4$	$\overline{R}_8$	$3.11 \cdot 10^{3}$
$\overline{R}_2$	$8.60 \cdot 10^{3}$	$\overline{R}_9$	$3.11\cdot 10^3$
$\overline{R}_3$	$1.96\cdot 10^2$	$\overline{R}_{10}$	$3.08\cdot 10^2$
$\overline{R}_4$	$9.78\cdot 10^2$	$\overline{R}_{11}$	$6.15\cdot 10^{1}$
$\overline{R}_5$	$6.00\cdot10^3$	$\overline{R}_{12}$	$2.70 \cdot 10^{3}$
$\overline{R}_6$	$6.00\cdot10^3$	$\overline{R}_{13}$	$5.74 \cdot 10^3$
$\overline{R}_7$	$11.36\cdot 10^3$		

Table 2

Values of the blood pressures in the reference configuration taken from Guidoboni et al. (2014b).

Pressure	Value	Pressure	Value
	[mmHg]		[mmHg]
$\overline{P}_0$	62.22	$\overline{P}_7$	24.25
$\overline{P}_1$	46.85	$\overline{P}_8$	22.13
$\overline{P}_2$	40.99	$\overline{P}_9$	20.01
$\overline{P}_3$	40.85	$\overline{P}_{10}$	19.80
$\overline{P}_4$	40.19	$\overline{P}_{11}$	19.76
$\overline{P}_5$	36.09	$\overline{P}_{12}$	17.92
$\overline{P}_6$	32.00	$\overline{P}_{13}$	14.00

Table 3

Resistance  $R_{i,j}$ , i = SCP, ICP, DCP, j = s, p (units: mmHg · s/mL) using the density data retrieved from Campbell et al. (2017) in the in parallel and in series configuration.

	In parallel	In series	
	[mmHg · s/mL]	[mmHg · s/mL]	
SCP	25560	2556	
ICP	32531	2501	
DCP	55052	5527	

Table 4

Computed volumetric blood flow rates  $Q_{i,p}^*$  and pressure drops  $\Delta P_{i,s}^*$  in each capillary plexus i =SCP, ICP, DCP, using the density data retrieved from Campbell et al. (2017) in the in parallel and in series configurations.

	In parallel	In series
	$Q_{i,p}^*[\mathrm{mLs}^{-1}]$	$\Delta P_{i,s}^*$ [mmHg]
SCP	$3.09\cdot 10^{-4}$	1.78
ICP	$2.43 \cdot 10^{-4}$	2.27
DCP	$1.43 \cdot 10^{-4}$	3.84

Table 5

Summary of the notation and the thickness (units:  $\mu$ m) of the tissue and vascular layers in the retina (Campbell et al., 2017; Terry et al., 2016).

	Retinal tissue layers			
(j)	Abbreviation	Layers Description	Thickness (µm)	
1	RPE	Retinal pigmented epithelium and outer segment of photoreceptors	15	
2	PH	Inner segment of photoreceptor layer	40	
3	ONL	Outer nuclear layer	90	
4	OPL	Outer plexiform layer	30	
5	INL	Inner nuclear layer	45	
6	IPL	Inner plexiform layer	45	
7	GCL	Ganglion cell and nerve fibre layer	70	
		Retinal vascular layers		
	Abbreviation	Layers Description	Thickness (µm)	
	SCP	Superficial capillary plexus	70	
	ICP	Intermediate capillary plexus	30	
	DCP	Deep capillary plexus	30	

Table 6

Parameters for the retinal oxygenation model.

Parameter	Unit	Value	References
Retinal surface $Q_{XY}$	cm <sub>2</sub>	10.9	-
Retinal parafoveal thickness $t_{\text{ret}}$	<i>µ</i> m	335	Terry et al. (2016)
Inner retinal thickness	<i>µ</i> m	190	Campbell et al. (2017), Terry et al. (2016)
Outer retinal thickness	<i>µ</i> m	145	Terry et al. (2016)
$O_2$ solubility coefficient in tissue $\alpha$	$\frac{mLO_2}{mL\;mmHg}$	$2.4 \cdot 10^{-5}$	Linsenmeier & Braun (1992)
Diffusivity of $O_2$ in tissue $D$	cm <sup>2</sup> /s	$1.4\cdot 10^{-5}$	Pogue et al. (2001)
Partial pressure of $O_2$ at the choroid $p_{ch}$	mmHg	80	Linsenmeier & Braun (1992)
Partial pressure of $O_2$ at the vitreous, $p_{vit}$	mmHg	20	-
Partial pressure of $O_2$ at half maximum consumption $K_{1/2}$	mmHg	2	Ganfield et al. (1970)
${ m O_2}$ capacity of red blood cells $c_o$	$\frac{\mathrm{cm}^3\mathrm{O}_2}{\mathrm{cm}^3}$	0.5	Arciero et al. (2008)
Discharge haematocrit, $H_D$	-	0.4	Arciero et al. (2008)
Saturation drop in the capillary plexuses in the reference condition:			
Total, $\Delta \overline{S}_{\mathrm{sat}}$	-	0.4	-
SCP, $\Delta \overline{S}_{sat}^{SCP}$	-	0.09	Evaluated from Chiaravalli (2018)
ICP, $\Delta \bar{S}_{sat}^{ICP}$	-	0.115	Evaluated from Chiaravalli (2018)
DCP, $\Delta \bar{S}_{\rm sat}^{\rm DCP}$	-	0.194	Evaluated from Chiaravalli (2018)
Volume of GCL, $V_{\rm GCL}$	$m^3$	$7.628 \cdot 10^{-8}$	Evaluated from Chiaravalli (2018)
Volume of ICP, $V_{ICP}$	$m^3$	$3.269 \cdot 10^{-8}$	Evaluated from Chiaravalli (2018)
Volume of DCP, $V_{\rm DCP}$	$m^3$	$3.269 \cdot 10^{-8}$	Evaluated from Chiaravalli (2018)